SIAM J. SCI. COMPUT.
Vol. 44, No. 4, pp. B996–B1017

UGKS-BASED IMPLICIT ITERATIVE METHOD FOR MULTISCALE NONEQUILIBRIUM FLOW SIMULATIONS*

XIAOCONG XU†, YAJUN ZHU†, CHANG LIU‡, AND KUN XU§

Abstract. The unified gas-kinetic scheme (UGKS) has been developed for rarefied and continuum flow simulations. To further enhance the computational efficiency of the implicit UGKS (IUGKS) [Y. Zhu, C. Zhong, and K. Xu, *J. Comput. Phys.*, 315 (2016), pp. 16–38] for the steady-state solution, a two-step IUGKS is proposed in this paper. The multiscale solution of the UGKS is determined by the integral solution of the kinetic model equation, which is composed of the Lagrangian integration of the equilibrium and the free particle transport of the nonequilibrium state. With the implicit evaluation of the macroscopic variables in the first iterative step, the integration of the equilibrium can be directly used in the flux calculation of macroscopic flow variables in the second iterative step. This is equivalent to including the viscous flux in the implicit scheme to accelerate the convergence of the solution instead of using the Euler flux in the iterative process of the original IUGKS. In the present IUGKS, the update of macroscopic flow variables is closely coupled with the implicit evolution of the gas distribution function. At the same time, to get a more accurate physical solution the full Boltzmann collision term has been incorporated into the current scheme through the penalty method. Different iterative techniques, such as lower-upper symmetric Gauss–Seidel and multigrid, are used for solving the linear algebraic system of coupled macroscopic and microscopic equations. The efficiency of the current IUGKS has reached an outstanding level among all implicit schemes for the kinetic equations in the literature. Several numerical examples are used to validate the performance of the IUGKS. Accurate solutions have been obtained efficiently in all cases from rarefied to continuum regimes and from low to hypersonic speed.

Key words. unified gas-kinetic scheme, implicit iterative method, Boltzmann collision operator, multigrid

MSC codes. 76P05, 76Pxx, 65M55

DOI. 10.1137/21M1421398

1. Introduction.

Gas dynamics can be modeled with a variable scale in different flow regimes. For the continuum flow, the well-known macroscopic governing equations for fluid dynamics are the Euler and Navier–Stokes (NS) equations, while in the rarefied regime, the kinetic equation on the particle mean free path scale becomes a reliable and effective description for nonequilibrium flow. The Boltzmann equation [1] is the fundamental equation for rarefied gas dynamics. Due to the complexity of the collision operator in the Boltzmann equation, some relaxation models, such as the Bhatnagar–Gross–Krook (BGK) model [2], the ellipsoidal statistical BGK model [3], and the Shakhov BGK (S-BGK) model [4], have been developed and are commonly used in both academic research and engineering application. Many kinetic solvers have been constructed for flow simulation, and most of them are required to have

*Submitted to the journal's Computational Methods in Science and Engineering section May 20, 2021; accepted for publication (in revised form) March 28, 2022; published electronically August 15, 2022.

https://doi.org/10.1137/21M1421398

Funding: This work was supported by the National Science Foundation of China 12172316 and by the National Numerical Windtunnel project.

†Department of Mathematics, The Hong Kong University of Science and Technology, Hong Kong, China (xxuay@connect.ust.hk, mazhuyajun@ust.hk).

‡Institute of Applied Physics and Computational Mathematics, No. 2, FengHao East Road, HaiDian District, Beijing 100094, China (liuchang@iapcm.ac.cn).

§Corresponding author. Department of Mathematics, The Hong Kong University of Science and Technology, Hong Kong, China; and HKUST Shenzhen Research Institute, Shenzhen 518057, China (makxu@ust.hk).

kinetic scale resolution to provide valid solutions, while, in the continuum regime, the kinetic method usually has poor performance due to the stiffness of the collision term and the use of discretized particle velocity space. The hydrodynamic flow solvers with the evolution of macroscopic flow variables become more accurate and efficient. The Chapman–Enskog procedure [5] gives the quasi-equilibrium distribution function in the continuum regime, which can be used directly in the construction of a hydrodynamic flow solver, such as the gas-kinetic scheme (GKS) for the NS solutions [6]. To simulate flows in all regimes, the unification of both kinetic and hydrodynamic modelings becomes necessary in the multiscale method [7].

To solve the kinetic equations, there are mainly two types of numerical methods, i.e., the stochastic methods and the deterministic methods. The direct simulation Monte Carlo (DSMC) [8] is the most popular stochastic method for high-speed rarefied flow. However, the particle method suffers from statistical noise, which makes it difficult in the low-speed flow simulation. The discrete velocity method (DVM) [9], as a deterministic method, is absent from noise but becomes extremely expensive due to the discretization of particle velocity space, especially for the high-speed and high-temperature flow. Both DSMC and conventional DVM are based on the operator splitting treatment for particle transport and collision. To keep the accuracy, the cell size–related numerical dissipation has to be properly controlled. In the above DSMC and DVM, the cell size and time step are restricted to be less than the particle mean free path and collision time in the explicit numerical evolution process. Under such a constraint, the computational cost will increase rapidly for the near continuum and continuum flow simulations. In order to design multiscale methods, asymptotic preserving (AP) schemes have been proposed in the past decades. This idea was originally used in neutron transport to capture the steady-state diffusion solution in the diffusive regime [10]. Later, the AP schemes have been constructed for a wide range of multiscale transport problems. Most AP schemes solve the microscopic equations only, and the macroscopic solutions will be obtained automatically from the kinetic solvers. Many of them are also based on micro-macro decomposition or the penalty technique for the capturing the Euler/NS limits in the continuum regimes [11, 12, 13]. Excellent AP schemes can be found in these review papers as well [14, 15, 16, 17].

Different from many AP schemes, the unified GKS (UGKS) solves both microscopic kinetic equation and macroscopic hydrodynamic equations. Based on the direct modeling of the cell size and time step scale, the UGKS has been proposed for multiscale simulation in all flow regimes [18, 19, 20, 21, 22]. Let $f = f(x, u, t)$ be the unknown gas distribution function, $g = g(x, u, t)$ be the reference gas distribution function, x be the position, u be the particle velocity, and τ be the local collision time. The original UGKS aims at solving the following type of kinetic equation

$$\frac{\partial f}{\partial t} + u \cdot \nabla_x f = \frac{g - f}{\tau}$$

by the finite volume method

$$f_{i,k}^{n+1} = f_{i,k}^{n} + \Delta t F_{i,k}^{n} + \frac{\Delta t}{2}\left(\frac{g_{i,k}^{n} - f_{i,k}^{n}}{\tau^{n}} + \frac{g_{i,k}^{n+1} - f_{i,k}^{n+1}}{\tau_{i,k}^{n+1}}\right)$$

with a proper flux function F^n, which accounts for the particle transport and collision within a time step. Here n is the time index, x is the position index, and i is the velocity index. For detailed construction of the flux function of UGKS, we refer to [18]

for more details. The key ingredient of the UGKS is that the numerical flux across the cell interface is constructed from the integral solution of the kinetic model equation, which couples the particle transport and collision in an evolution process and uses the accumulating solution of particles' collision within a numerical time step for the update of the solution. In other words, the local flow physics recovered by the UGKS is determined by the ratio of particle collision time and the numerical time step, i.e., the cell's Knudsen number. The UGKS has an asymptotic limit to the NS solution in the continuum flow regime without the kinetic scale restriction on the time step and cell size.

For the steady-state calculation, many implicit schemes for the kinetic equations have been developed for fast convergence. The high-order and low-order method [23, 24] couples the high-order kinetic equation and a low-order fluid moment equation, targeting fast convergence in both continuum and rarefied regimes. With a similarly coupled system, the recently developed general synthetic iterative scheme [25, 26] shows a promising efficiency in multiscale flow simulation, where the constitutive relations of NS shear stress and heat conduction are explicitly used to guide the convergence of macroscopic solutions. For the UGKS, the implicit scheme constructs the flux function F at the $n+1$ step, which reads as

$$f_{i,k}^{n+1} = f_{i,k}^{n} + \Delta t F_{i,k}^{n+1} + \Delta t \left(\frac{g_{i,k}^{n+1} - f_{i,k}^{n+1}}{\tau_{i,k}^{n+1}} \right).$$

The problem boils down to the construction of $F_{i,k}^{n+1}$ and the method for solving the implicit system of equations. The detailed derivation will be introduced in section 3. Standard implicit techniques in CFD, such as lower-upper symmetric Gauss–Seidel (LU-SGS) and multigrid, can also be incorporated in implicit UGKS (IUGKS) [27, 28, 29], which made a significant improvement in convergence for the steady-state solution.

The present work is targeting the further improvement of IUGKS, where an even closer coupling of both macroscopic and microscopic evolution equations will be developed implicitly. We still start from the two aspects, the construction of $F_{i,k}^{n+1}$ and the method for solving the implicit system of equations, to improve the efficiency of IUGKS. From the perspective of the construction of $F_{i,k}^{n+1}$, we take the NS dissipative terms into account and then construct a two-step IUGKS. On the other hand, to solve the implicit system of equations efficiently, we equip the IUGKS with a multigrid solver. A comparative study of efficiency will be presented from different algebraic iterative methods. To treat the collision term in a fully implicit way, the macroscopic governing equations will be solved implicitly first for the prediction of the equilibrium state. Afterward, based on the predicted conservative flow variables, the evolution equation of the distribution function forms a diagonal matrix system. Then both the matrix systems derived from implicit macroscopic equations and implicit microscopic equations are solved iteratively using the LU-SGS method with a multi-grid acceleration. In addition, to achieve a reliable physical solution in the highly rarefied regime, the full Boltzmann collision operator is integrated into the IUGKS for the steady-state solutions.

The paper is organized as follows. In section 2, the explicit UGKS scheme is briefly introduced. In section 3, a general framework of IUGKS is presented and described in detail, which includes the discretization of the full Boltzmann collision operator and the two-step acceleration technique. The numerical procedures for solving algebraic systems raised from IUGKS for the evolution of microscopic and macroscopic equa-

tions will be discussed in section 4. The numerical tests, including low-speed Couette flow, the Fourier flow, lid-driven cavity flow, and the high-speed flow around a square cylinder, will be presented in section 5. The conclusion will be drawn in section 6.

2. Kinetic equation and UGKS.

2.1. Kinetic equation. The kinetic equations describe the time evolution of the probability distribution function (PDF) or velocity distribution function on the kinetic scale. The kinetic equation models both particle transport and collision in the following form:

$$\partial_t f + u \cdot \nabla_x f = Q, \tag{1}$$

where $f = f(x, t, u)$ is the velocity PDF, x is the spatial position, t is the time, and u is the particle velocity. Here x, u, W are vectors in $\mathbb{R}^3$. The collision term Q can be modeled by the nonlinear Boltzmann collision term $Q(f, f)$ and the kinetic relaxation process. The Boltzmann collision term takes the form

$$Q(f,f)(u) = \int_{\mathbb{R}^3}\int_{\mathbb{S}^2} B(|u-u_*|,\sigma)\left[f(u_*')f(u') - f(u_*)f(u)\right] d\sigma du_*, \tag{2}$$

where $B(|u-u_*|,\sigma)$ is the collision kernel. The numerical evaluation of the nonlinear Boltzmann collision operator is highly expensive due to its fivefold integration form. In order to simplify the formulation, the relaxation type of collision operator is considered here, such as the S-BGK model

$$Q(f) = \frac{g-f}{\tau}, \tag{3}$$

where $\tau = \mu/p$ is the local mean collision time computed from the dynamic viscosity coefficient μ and the pressure p. The equilibrium state g takes the form of

$$g = g^M\left[1 + (1-\mathrm{Pr})c\cdot q\left(\frac{c^2}{RT} - 5\right)\right], \tag{4}$$

and g^M is the Maxwellian distribution

$$g^M = \frac{\rho}{(2\pi RT)^{3/2}}\exp\left(-\frac{c^2}{2RT}\right), \tag{5}$$

where ρ is the mass density, R is the specific gas constant, Pr is the Prandtl number, $c = u - U$ is the peculiar velocity with U the macroscopic flow velocity, and q is the heat flux. The relation between distribution function and macroscopic conservative flow variables is defined as

$$W = \int f\psi du. \tag{6}$$

Here, $\psi = \left[1, u, \frac{1}{2}|u|^2\right]^T$ is the vector of collision invariants, and $W = [\rho, \rho U, \rho E]^T$ is the vector of conservative flow variables. The pressure tensor $\mathbf{P}$ and the heat flux q can be also calculated from the PDF by

$$\mathbf{P} = \int ccf du, \quad q = \frac{1}{2}\int c|c|^2 f du. \tag{7}$$

Based on the kinetic equation, a UGKS has been developed for capturing both kinetic and hydrodynamic solutions in the corresponding regime [18].

2.2. UGKS. In this subsection, the explicit UGKS is briefly introduced. The UGKS takes direct modeling of flow physics on the discretization scales, i.e., the time step and cell size. In the framework of a finite volume method, if the trapezoidal rule is used for the collision term, the conservation of the gas distribution function can be described as

(8)
$$f_{i,k}^{n+1} = f_{i,k}^{n} - \frac{1}{V_i}\sum_{j\in N(i)} S_{ij}\int_{t^n}^{t^{n+1}} u_{k,N} f_{ij,k}(t)dt + \frac{\Delta t}{2}\left(\frac{g_{i,k}^{n} - f_{i,k}^{n}}{\tau_i^n} + \frac{g_{i,k}^{n+1} - f_{i,k}^{n+1}}{\tau_i^{n+1}}\right),$$

where $f_{i,k}^n$ and $f_{i,k}^{n+1}$ are spatially averaged distribution functions of cell i at particle velocity u_k and at time t^n and t^{n+1}, respectively. $N(i)$ is the index set of the neighbors of cell i, and ij denotes the interface between cells i and j. V_i is the volume of cell i, S_{ij} is the area of the interface ij, $u_{k,N}$ is the normal projection of particle velocity u_k along the cell interface, and $f_{ij,k}(t)$ is a time-dependent distribution function on the interface ij at particle velocity u_k.

Multiplying by the collision invariants and applying a quadrature rule in velocity space, the conservation laws of macroscopic flow variables can be obtained from (8):

$$W_i^{n+1} = W_i^n - \frac{1}{V_i}\sum_{j\in N(i)} S_{ij}\left(\sum_k \int_{t^n}^{t^{n+1}} u_{k,n} f_{ij,k}(t)\psi_k dt\right). \tag{9}$$

Here, $\psi_k = [1, u_k, \frac{1}{2}|u_k|^2]^T$. In order to evolve the above discretized equations, a time-dependent distribution function $f_{ij,k}(t)$ has to be constructed. Based on the integral solution of (1), a multiscale $f_{ij,k}(t)$ can be modeled as

(10)
$$\begin{aligned} f_{ij,k}(t) &= f\left(x_{ij}, t, u_k\right) \\ &= \frac{1}{\tau}\int_{t^n}^{t} g\left(x', t', u_k\right) e^{-\left(t-t'\right)/\tau} dt' + e^{-(t-t^n)/\tau} f\left(x_{ij} - u_k\left(t-t^n\right), t^n, u_k\right), \end{aligned}$$

where $x' = x_{ij} - u_k(t-t')$ is the particle trajectory.

For a second-order spatial accuracy, the initial distribution function around the cell interface ij can be approximated by

$$f_{0,k}\left(x\right) = f\left(x, t^n, u_k\right) = \begin{cases} f_{ij,k}^i + \sigma_i^n \cdot x, & n_{ij}\cdot x < 0, \\ f_{ij,k}^j + \sigma_j^n \cdot x, & n_{ij}\cdot x \geq 0, \end{cases} \tag{11}$$

where $f_{ij,k}^i$ and $f_{ij,k}^j$ are the reconstructed initial distribution functions on both sides of the cell interface ij, and n_{ij} is the unit normal vector of the cell interface ij. $\sigma = \nabla_x f$ is the spatial gradient of the initial distribution function, which is nonlinearly limited in case of discontinuity. In this paper, we use the least square reconstruction to obtain the gradient. In addition, the equilibrium state is approximated by Taylor expansion,

$$g_k\left(x,t\right) = g\left(x,t,u_k\right) = g_{0,k} + x\cdot\nabla_x g_{0,k} + t\partial_t g_{0,k}, \tag{12}$$

where $g_{0,k}$ is the initial equilibrium at the cell interface ij, and $\nabla_x g_{0,k}$ and $\partial_t g_{0,k}$ are the spatial and temporal gradients of the initial equilibrium state. The detailed calculation for these terms can be found in previous literature [18]. Applying (11) and (12) to (10), the time-dependent distribution function $f_{ij,k}(t)$ can be computed by

$$f_{ij,k}(t) = q_1 g_{0,k} + q_2 u_k\cdot\nabla_x g_{0,k} + q_3\partial_t g_{0,k} + q_4 f_{0,k} + q_5 u_k\cdot\nabla_x f_{0,k}, \tag{13}$$

where the coefficients q are

$$
\begin{aligned}
q_1 &= 1 - e^{-t/\tau}, \\
q_2 &= \tau\left(e^{-t/\tau} - 1\right) + te^{-t/\tau}, \\
q_3 &= t - \tau + \tau e^{-t/\tau}, \\
q_4 &= e^{-t/\tau}, \\
q_5 &= -te^{-t/\tau}.
\end{aligned} \tag{14}
$$

Rewrite (13) into the following form:

$$
\begin{aligned}
f_{ij,k}(t) &= g_{ij,k} + q_2 u_k \cdot \nabla_x g_{ij,k} + q_3 \partial_t g_{ij,k} + q_4\left(f_{ij,k} - g_{ij,k}\right) + q_5 u_k \cdot \nabla_x f_{ij,k} \\
&\triangleq \tilde{g}_{ij,k} + \tilde{f}_{ij,k},
\end{aligned} \tag{15}
$$

where $\tilde{g}_{ij,k} \triangleq g_{ij,k} + q_2 u_k \cdot \nabla_x g_{ij,k} + q_3 \partial_t g_{ij,k}$ is related to the evolution of the equilibrium state. This term gives the NS distribution function from the integration of the equilibrium state as $\Delta t >> \tau$. $\tilde{f}_{ij,k} \triangleq q_4\left(f_{ij,k} - g_{ij,k}\right) + q_5 u_k \cdot \nabla_x f_{ij,k}$ is related to the particle free transport of the initial nonequilibrium state. Note that under this arrangement, the flux related to $\tilde{f}_{ij,k}$ will mainly contribute to the nonequilibrium transport, which plays an important role in the rarefied regime. The above formulation will be used in the construction of the IUGKS.

As long as the time-dependent distribution function $f_{ij,k}(t)$ is obtained, the flux term in (8) and (9) can be computed. Then we can update the averaged distribution function $f_{i,k}^{n+1}$ and macroscopic flow variables W_i^{n+1} in each cell.

3. General framework of the IUGKS. For steady-state calculation, a finite volume implicit discretization of (1) can be written as

$$
\frac{f_{i,k}^{n+1} - f_{i,k}^{n}}{\Delta t} + \frac{1}{V_i}\sum_{j \in N(i)} S_{ij} u_{k,N} f_{ij,k}^{n+1} = \frac{\tilde{g}_{i,k}^{n+1} - f_{i,k}^{n+1}}{\tau_i^{n+1}}. \tag{16}
$$

Here, the implicit numerical time step Δt is introduced to improve the stability of the scheme. In the above equation, a prediction step should be carried out first to obtain an approximate equilibrium state $\tilde{g}^{n+1}$ so that the collision term can be treated implicitly. For simplicity, the formulations in this section are presented for two-dimensional cases, and the extension to three-dimensional cases would be straightforward.

3.1. Prediction step for $\tilde{g}^{n+1}$. Taking moments of (16), we can obtain the implicit governing equations of macroscopic flow variables, i.e.,

$$
\frac{\tilde{W}_i^{n+1} - W_i^{n}}{\Delta t} + \frac{1}{V_i}\sum_{j \in N(i)} S_{ij} F_{ij}^{n+1} = 0, \tag{17}
$$

where F_{ij}^{n+1} are the fluxes for conservative variables at the interface ij. Subtracting the fluxes at time t^n from both sides, the governing equations could be rewritten as

$$
\frac{1}{\Delta t}\Delta W_i^{n+1} + \frac{1}{V_i}\sum_{j \in N(i)} S_{ij} \Delta F_{ij}^{n+1} = -\frac{1}{V_i}\sum_{j \in N(i)} S_{ij} F_{ij}^{n}, \tag{18}
$$

where $\Delta W_i^{n+1} = \tilde{W}_i^{n+1} - W_i^n$ and $\Delta F_{ij}^{n+1} = F_{ij}^{n+1} - F_{ij}^n$. In order to solve (18), the fluxes on the left-hand side will be approximated by the Euler equation–based fluxes, which will lead to a matrix-free algorithm,

(19)
$$\Delta F_{ij}^{n+1} \approx \frac{1}{2}\left[T_i^{n+1} + T_j^{n+1} + \Gamma_{ij}\left(W_i^{n+1} - W_j^{n+1}\right)\right] - \frac{1}{2}\left[T_i^n + T_j^n + \Gamma_{ij}\left(W_i^n - W_j^n\right)\right],$$

where T is the Euler flux, which can be determined by the conservative variables

(20)
$$T = \begin{bmatrix} \rho U_x \\ \rho U_x^2 + p \\ \rho U_x U_y + p \\ (\rho E + p) U_x \end{bmatrix} n_x + \begin{bmatrix} \rho U_y \\ \rho U_x U_y + p \\ \rho U_y^2 + p \\ (\rho E + p) U_y \end{bmatrix} n_y.$$

Here, $[n_x, n_y]^T$ is the unit normal vector along the interface, and p is the pressure. The factor Γ_{ij} satisfies

(21)
$$\Gamma_{ij} \geq \Lambda_{ij} = |U_{ij} \cdot n_{ij}| + a_s,$$

where Λ_{ij} represents the spectral radius of the Jacobian of the Euler flux, which can be evaluated by the macroscopic velocity U_{ij} and the speed of sound a_s at the interface ij. Moreover, as stated in the previous literature [30], a stable factor s_{ij} related to the viscosity coefficient can be introduced into the calculation of Γ_{ij}:

(22)
$$\Gamma_{ij} = \Lambda_{ij} + s_{ij} = \Lambda_{ij} + \frac{2\nu}{\Delta l}.$$

The above flux is the so-called Lax–Friedrichs flux, and in order to simplify the notations, we define

$$\begin{aligned} A_i\left(W_i\right) &\triangleq \frac{W_i}{\Delta t} + \frac{1}{V_i}\sum_{j \in N(i)} S_{ij} F_{LF}\left(W_i, W_j\right) \\ &= \frac{W_i}{\Delta t} + \frac{1}{V_i}\sum_{j \in N(i)} S_{ij}\frac{1}{2}\left[T_i + T_j + \Gamma_{ij}\left(W_i - W_j\right)\right]. \end{aligned}$$

Then the evolution equations can be rewritten as

(23)
$$A_i\left(\tilde{W}_i^{n+1}\right) = R_i^n + A_i\left(W_i^n\right), \quad R_i^n = -\frac{1}{V_i}\sum_{j \in N(i)} S_{ij} F_{ij}^n,$$

where F_{ij}^n are the fluxes calculated from the time-dependent distribution function $f_{ij,k}(t)$ in (16), which reads as

(24)
$$F_{ij}^n = \frac{1}{\Delta t_s}\sum_k \int_0^{\Delta t_s} u_{k,N} f_{ij,k}(t)\psi_k dt.$$

Here, the sum over k is the numerical procedure for integration over the velocity space. Δt_s is a small time step to determine the local physics scale, which is calculated the same as that in the explicit UGKS by the stability condition

(25)
$$\Delta t_s = \alpha \min \frac{\Delta x}{\max |u_k|},$$

where Δx is the mesh size and α is the CFL number. It should be noticed that the time step Δt_s is different from the implicit numerical time step Δt. In the IUGKS, Δt_s can be regarded as a cell size–related time step to decide the local physical solution in the corresponding scale by adjusting the combination of equilibrium and nonequilibrium distribution function, and it is the time step to average the numerical fluxes for controlling convergent steady-state solution, while Δt is the pseudo–time step to increase the convergence stability for the steady-state solution.

At the steady state, the Lax–Friedrichs flux $A_i(\cdot)$ on the left- and right-hand side of (23) will be canceled, and the convergent solution will be completely controlled by

$$\frac{1}{V_i}\sum_{j\in N(i)} S_{ij}F_{ij}^n = 0, \tag{26}$$

which ensures identical steady solutions as the explicit UGKS.

By solving (23), we can get the prediction macroscopic conservative variables $\tilde{W}^{n+1}$, and therefore $\tilde{g}^{n+1}$ can be obtained simultaneously. The detail for solving (23) by using a matrix-free algorithm will be given later.

3.2. Solving the microscopic system. With the predicted equilibrium state $\tilde{g}^{n+1}$, by introducing $\Delta f^{n+1} = f^{n+1} - f^n$ and then rearranging the terms, (16) can be rewritten in a delta-form

$$\frac{1}{\Delta t}\Delta f_{i,k}^{n+1} + \frac{1}{V_i}\sum_{j\in N(i)} u_{k,N}S_{ij}\Delta f_{ij,k}^{n+1} = \frac{\tilde{g}_i^{n+1} - f_i^n}{\tilde{\tau}_i^{n+1}} - \frac{1}{V_i}\sum_{j\in N(i)} u_{k,n}S_{ij}f_{ij,k}^n. \tag{27}$$

Here $\tilde{\tau}^{n+1}$ can be also obtained from the predicted macroscopic variables. Since different algorithms to compute the implicit fluxes at the left-hand side of (27) will not affect the final convergent solutions, the first-order upwind scheme is adopted here to compute $\Delta f_{ij,k}^{n+1}$, which reads as

$$\begin{aligned}\Delta f_{ij,k}^{n+1} &= \frac{1}{2}\left(\Delta f_{i,k}^{n+1} + \Delta f_{j,k}^{n+1}\right) + \frac{1}{2}\operatorname{sign}(u_k\cdot n_{ij})\left(\Delta f_{i,k}^{n+1} - \Delta f_{j,k}^{n+1}\right),\\ &= \frac{1}{2}\left[1+\operatorname{sign}(u_{k,n})\right]\Delta f_{i,k}^{n+1} + \frac{1}{2}\left[1-\operatorname{sign}(u_{k,n})\right]\Delta f_{j,k}^{n+1}.\end{aligned} \tag{28}$$

Inserting (28) into (27), we can get a linear system,

$$D_{i,k}\Delta f_{i,k}^{n+1} + \sum_{j\in N(i)} D_{j,k}\Delta f_{j,k}^{n+1} = (\mathrm{RHS})_{i,k}^n, \tag{29}$$

where

$$\begin{aligned} D_{i,k} &= \frac{1}{\Delta t} + \frac{1}{\tilde{\tau}_i^{n+1}} + \frac{1}{2V_i}\sum_{j\in N(i)} u_{k,N}S_{ij}\left[1+\operatorname{sign}(u_{k,N})\right],\\ D_{j,k} &= \frac{1}{2V_i}u_{k,N}S_{ij}\left[1-\operatorname{sign}(u_{k,N})\right],\\ (\mathrm{RHS})_{i,k}^n &= \frac{\tilde{g}_{i,k}^{n+1} - f_{i,k}^n}{\tilde{\tau}_i^{n+1}} - \frac{1}{V_i}\sum_{j\in N(i)} S_{ij}u_{k,N}f_{ij,k}^n. \end{aligned} \tag{30}$$

These terms $D_{i,k}$ and $D_{j,k}$ will be the entries of a block diagonal matrix. Once the steady state is reached, $\Delta f_{i,k}^{n+1}$ will go to zero, and the steady state should satisfy $(\mathrm{RHS})_{i,k}^n = 0$.

3.3. Extension to full Boltzmann collision operator. Consider the nonlinear Boltzmann in the dimensionless form, which reads as

$$\frac{\partial f}{\partial t} + u \cdot \nabla_x f = \frac{1}{\mathrm{Kn}} Q(f, f). \tag{31}$$

where the collision operator Q is a bilinear operator, which can be written as

$$Q(g, f)(u) = \int_{\mathbb{R}^3} \int_{\mathbb{S}^2} B(|u - u_*|, \sigma) \left[g(u'_*) f(u') - g(u_*) f(u) \right] d\sigma du_*. \tag{32}$$

Here (u, u_*) and (u', u'_*) are the velocity pairs before and after a collision. By the momentum and energy conservation, one can show that (u', u'_*) can be represented in terms of (u, u_*) as

$$u' = \frac{u + u_*}{2} + \frac{|u - u_*|}{2}\sigma, \quad u'_* = \frac{u + u_*}{2} - \frac{|u - u_*|}{2}\sigma \tag{33}$$

with $\sigma = (u' - u'_*)/|u' - u'_*|$ varying in the unit sphere $\mathbb{S}^2$. The collision kernel $B(|u - u_*|, \sigma)$ is a nonnegative function depending only on $|v - v_*|$ and the cosine of the deflection angle θ. In the following numerical examples, we consider a simplified collision kernel,

$$B(|u - u_*|, \sigma) = C_\alpha |u - u_*|^\alpha, \tag{34}$$

which is the so-called variable hard sphere (VHS) model. The penalization technique [31] is used in the construction of our numerical scheme, which can be formulated as

$$\begin{aligned} &\frac{f_{i,k}^{n+1} - f_{i,k}^n}{\Delta t} + \frac{1}{V_i} \sum_{j \in N(i)} S_{ij} u_{k,N} f_{ij,k}^{n+1} = S_{i,k}^n + \frac{\tilde{g}_{i,k}^{n+1} - f_{i,k}^{n+1}}{\tau_i^{n+1}}, \\ &S_{i,k}^n = \frac{\left[\mathcal{Q}\left(f_i^n, f_i^n\right) \right]_k}{\mathrm{Kn}} - \frac{g_{i,k}^n - f_{i,k}^n}{\tau_i^n}. \end{aligned} \tag{35}$$

This is an implicit scheme, and the collision operator is solved by the fast spectral method explicitly [32, 15, 33]. In the continuum regime, the predicted $\tilde{g}_i^{n+1}$ in the penalized term could boost the convergence of the implicit scheme. In the framework of the IUGKS, the only difference with the above procedure is that the $(\mathrm{RHS})_{i,k}^n$ becomes

$$(\mathrm{RHS})_{i,k}^n = \frac{\tilde{g}_{i,k}^{n+1} - f_{i,k}^n}{\tilde{\tau}_i^{n+1}} - \frac{1}{V_i} \sum_{j \in N(i)} S_{ij} u_{k,N} f_{ij,k}^n + S_{i,k}^n. \tag{36}$$

Compare this with the AP scheme [15], which can be written as

$$\begin{aligned} &\frac{f_{i,k}^{n+1} - f_{i,k}^n}{\Delta t} + \frac{1}{V_i} \sum_{j \in N(i)} S_{ij} u_{k,N} f_{ij,k}^n = S_{i,k}^n + \frac{g_{i,k}^{n+1} - f_{i,k}^{n+1}}{\tau_i^{n+1}}, \\ &S_{i,k}^n = \frac{\left[\mathcal{Q}\left(f_i^n, f_i^n\right) \right]_k}{\mathrm{Kn}} - \frac{g_{i,k}^n - f_{i,k}^n}{\tau_i^n}. \end{aligned} \tag{37}$$

We can see the main difference between the current scheme (35) and the AP scheme is the calculation of the flux function. The AP scheme evaluates the flux function explicitly, while in the current scheme we evaluate it implicitly.

3.4. Two-step iteration for acceleration. The development of a new acceleration method is based on two observations. First, in the IUGKS, the microscopic system is mainly driven by the predicted $\tilde{g}^{n+1}$. Therefore, if we can have a good prediction (closer to the steady solution), the computational cost can be much reduced, especially in the continuum regime. The second observation is that in the continuum regime, the UGKS flux is dominated by $\tilde{g}_{ij,k}$ in (15). Instead of updating the $f_{ij,k}$ in each discrete velocity point and then using numerical quadrature to get the macroscopic flux, the macroscopic flux related to the analytical part $\tilde{g}_{ij,k}$ can be computed with relatively low computational cost by using the analytical formulations.

In the previous study, in the continuum regime, the left-hand side of the IUGKS is driven by the Euler flux. Based on the multiscale property of the UGKS flux, we can naturally take the viscosity flux into account and use the viscous solution to boost the convergence of IUGKS. Similar consideration can be found in Yuan, Liu, and Zhong [34].

Consequently, we can take one more prediction step for $\tilde{g}^{n+1}$ in the computational procedure. More specifically, by the first step iteration in solving (23) for macroscopic variables, an equilibrium $\tilde{g}^*$ term in (16) can be predicted. Then, we can update the macroscopic flux by

$$F_{ij}^{n,*} = \frac{1}{\Delta t_s}\int_0^{\Delta t_s} \langle u \cdot n \psi \tilde{g}_{ij,k}^* \rangle dt + \frac{1}{\Delta t_s}\sum_k \int_0^{\Delta t_s} u_{k,n} \tilde{f}_{ij,k}^n \psi_k dt. \tag{38}$$

The evolution equations for the second step iteration can be written as

$$A_i\left(\tilde{W}_i^{n+1}\right) = R_i^{n,*} + A_i\left(W_i^*\right), \quad R_i^{n,*} = -\frac{1}{V_i}\sum_{j\in N(i)} S_{ij} F_{ij}^{n,*}, \tag{39}$$

where W_i^* is the conservative calculated by $\tilde{g}^*$.

So far, a brief summary of the present implicit scheme can be given, and the major steps are listed as follows:

1. Get the predicted $\tilde{g}^{n+1}$ by iterating (23) and (39) in order from initial W^n.
2. Get the Δf^{n+1} by solving (29) with the predicted $\tilde{g}^{n+1}$ and initial f^n.
3. Update the distribution function f^{n+1} by $f^{n+1} = f^n + \Delta f^{n+1}$, and get the updated macro conservative variables from (6).
4. Repeat the steps 1 to 3 until satisfying the convergence criterion.

4. Iterative methods for solving coupled macro-micro system. An improved IUGKS will be presented to solve the implicit system. For each iteration of (39), we are solving (23) with the refreshed F_{ij} and W_i at the right-hand side. In the following, the detailed methods for solving (23) and (29) will be discussed.

4.1. LU-SGS method. Subtracting $A_i(W_i^n)$ on both sides of (23) and performing the Taylor approximation, we can obtain

$$\frac{\partial A}{\partial W}\Delta W^n = R^n. \tag{40}$$

The Jacobian matrix-splitting method in [35] can be used to solve the above system. However, the computation of the Jacobian matrix requires additional storage. The inverse linearization can be used to eliminate the computation of the Jacobian matrix

[36], in which the following approximation is adopted:

$$\begin{aligned}\frac{\partial A_i}{\partial W_i}\Delta W_i^n &\approx A_i\left(W_i^n+\Delta W_i^n\right)-A_i\left(W_i^n\right)\\ &=\left(\frac{1}{\Delta t}+\frac{1}{2}\sum_{j\in N(i)}S_{ij}\Gamma_{ij}\right)\Delta W^n\\ &+\ \frac{1}{2}\sum_{j\in N(i)}S_{ij}\left[T\left(W_j^n+\Delta W_j^n\right)-T\left(W_j^n\right)-\Gamma_{ij}\Delta W_j^n\right].\end{aligned}\tag{41}$$

Therefore, the LU-SGS method for the algebraic system (40) and (41) can be described by a forward step

$$\Delta W_i^*=D_i^{-1}\left(R_i^n-\frac{1}{2}\sum_{j\in L(i)}S_{ij}\left[T\left(W_j^n+\Delta W_j^*\right)-T\left(W_j^n\right)-\Gamma_{ij}\Delta W_j^*\right]\right)\tag{42}$$

and a backward step

$$\Delta W_i^n=\Delta W_i^*-D_i^{-1}\left(\frac{1}{2}\sum_{j\in U(i)}S_{ij}\left[T\left(W_j^n+\Delta W_j^n\right)-T\left(W_j^n\right)-\Gamma_{ij}\Delta W_j^n\right]\right),\tag{43}$$

where D_i is the diagonal element of the matrix

$$D_i=\frac{1}{\Delta t}+\frac{1}{2}\sum_{j\in N(i)}S_{ij}\Gamma_{ij}.\tag{44}$$

Here, $L(i)$ is the index set of the neighboring cells of cell i occupying the lower triangular part of the matrix, and $U(i)$ is the index set of the neighboring cells of cell i occupying the upper triangular part of the matrix. The numbering of the index is essential to the LU-SGS sweeping, and bad numbering may lead to local degeneration from Gauss–Seidel iteration to Jacobian iteration.

4.2. Multigrid method. In this subsection, the geometry type of multigrid method [37] for solving the macro-system (23) and micro-system (29) will be implemented and used in the calculation of two-dimensional numerical examples.

Firstly, the restriction and interpolation operator should be properly defined to connect different levels of mesh [28]. The restriction operator I_h^H, which maps the quantities from a fine mesh to a coarse mesh, can be naturally defined as the average quantities of all the related cells in the fine mesh. Specifically, for a quantity Q_h in a fine mesh, the restricted quantity Q_H in a coarse mesh can be calculated as

$$Q_{H,i}=I_h^H(\{Q_{h,j},j\in S(i)\})=\frac{\sum_{j\in S(i)}Q_{h,j}V_{h,j}}{\sum_{j\in S(i)}V_{h,j}},\tag{45}$$

where the subscripts i,j denote the quantities in cell i,j, $S(i)$ is the index set of the related cells, and V is the volume of the cell. The interpolation operator I_H^h is a bilinear interpolation operator. For the rectangular mesh as shown in Figure 1, let $(x_1,y_1),(x_1,y_2),(x_2,y_1),(x_2,y_2)$ be the four corner points of the current cell; I_H^h is defined as

$$Q_{h,i}=I_H^h(\{Q_{H,j},j\in S(i)\})=\frac{\sum_{j\in S(i)}w_jQ_{H,j}}{\sum_{j\in S(i)}w_j},\tag{46}$$

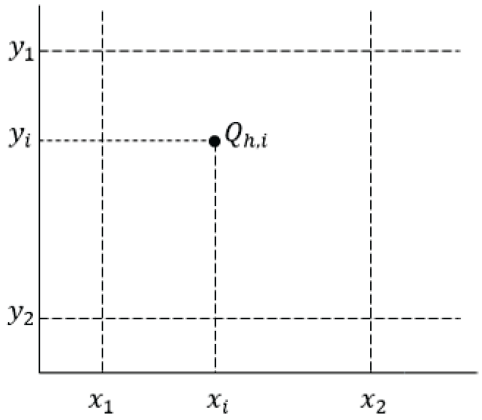

FIG. 1. *Bilinear interpolation.*

and

$$\begin{aligned} w_1 &= (x_2 - x_i)(y_2 - y_i), \\ w_2 &= (x_i - x_1)(y_2 - y_i), \\ w_3 &= (x_2 - x_i)(y_i - y_1), \\ w_4 &= (x_i - x_1)(y_i - y_1). \end{aligned} \tag{47}$$

Here, (x_i, y_i) is the center coordinate of cell i.

After these two operations are determined, the multigrid method for solving (23) and (29) can be constructed. For simplicity, the basic two-grid cycle method will be discussed, and the multiple V-cycle can be done recursively.

4.3. Multigrid method for macro-system. Since (23) is a nonlinear system, the full approximation scheme [38] will be used to solve this system. The algorithm for a two-grid cycle can be described as follows.

- Presmoothing: perform ν_1 times LU-SGS to get an approximate solution $W^*_{h,i}$ of (23), and then compute the residual by $r_{h,i} = R^n_{h,i} + A(W^n_{h,i}) - A(W^*_{h,i})$.
- Restriction: restrict $W^*_{h,i}$ and $r_{h,i}$ to a coarse grid by $r_{H,i} = I^H_h(\{r_{h,j}, j \in S(i)\})$ and $W^*_{H,i} = I^H_h(\{W^*_{h,j}, j \in S(i)\})$.
- Smoothing: perform ν_2 times LU-SGS to get an approximation solution $W^{**}_{H,i}$ of the coarse grid problem $A(W_{H,i}) = r_{H,i} + A\left(W^*_{H,i}\right)$.
- Correction: compute the error $e_{H,i}$ in the coarsegrid by $e_{H,i} = W^{**}_{H,i} - W^*_{H,i}$, and then correct the approximation solution in the fine grid by $W^*_{h,i} = W^*_{h,i} + I^h_H(\{e_{H,j}, j \in S(i)\})$.
- Postsmoothing: perform ν_3 times LU-SGS to get the final solution $W^{n+1}_{h,i}$ of (23) with the initial guess $W^*_{h,i}$.

4.4. Multigrid method for micro-system. For the linear system (29), the two-grid correction scheme can be summarized as follows.

- Presmoothing: perform γ_1 times symmetric Gauss–Seidel (SGS) to get an approximate solution $\Delta f^*_{h,\{i,k\}}$ of (29), and then compute the residual by

$$r_{h,\{i,k\}} = (\mathrm{RHS})_{h,\{i,k\}} - \left(D_{h,\{i,k\}} \Delta f^*_{h,\{i,k\}} + \sum_{j \in N(i)} D_{h,\{j,k\}} \Delta f^*_{h,\{j,k\}} \right).$$

- Restriction: restrict $\Delta f^*_{h,\{i,k\}}$, $r_{h,\{i,k\}}$, and $D_{h,\{i,k\}}$ to a coarse grid by the restriction operator I_h^H.
- Smoothing: perform γ_2 times SGS to get a solution of the residual equation

$$D_{H,\{i,k\}}\Delta e_{H,\{i,k\}} + \sum_{j\in N(i)} D_{H,\{j,k\}}\Delta e_{H,\{j,k\}} = r_{H,\{i,k\}}.$$

- Correction: correct the approximation solution in the fine grid by $\Delta f^*_{h,\{i,k\}} = \Delta f^*_{h,\{i,k\}} + I_H^h(\{e_{H,\{i,k\}}, j \in S(i)\})$,
- Postsmoothing: perform γ_3 times SGS to get the final solution $\Delta f^{n+1}_{h,\{i,k\}}$ of (23) with the initial guess $\Delta f^*_{h,\{i,k\}}$.

The two-step IUGKS with single grid is just a reduction of the two-step IUGKS with multigrid, where the presmoothing and postsmoothing steps are kept. Since the nonlinear system may take more steps to get an accurate solution, the smoothing times ν_i for the nonlinear system are taken to be more than the smoothing times γ_i for the linear system. As demonstrated in [39], common choices are $\gamma_1 + \gamma_3 \le 3$ in practice. In this paper, we set $\nu_1 = 10$, $\nu_2 = 10$, $\nu_3 = 5$ and $\gamma_1 = 2$, $\gamma_2 = 2$, $\gamma_3 = 1$.

5. Numerical validation. In this section, several numerical examples will be presented to validate the accuracy and efficiency of the IUGKS, including the extension to the full Boltzmann collision operator. For two-dimensional cases, we will investigate the efficiency of three different IUGKSs, which include the original IUGKS [27], the two-step IUGKS, and the two-step IUGKS with a V-cycle multigrid solver.

5.1. Couette flow. The first case is the planar Couette flow for argon gas with $\omega = 0.81$. The full Boltzmann collision operator is considered in this case. The Knudsen number is defined by $\mathrm{Kn} = \mu_0\sqrt{2\pi RT_0}/(2p_0L)$, where T_0 is the reference temperature, ρ_0 is the reference density, μ_0 is the viscosity, $p_0 = \rho_0 RT_0$ is the pressure, and L is the characteristic length. The nondimensional quantities are used in the numerical simulation. Therefore, without loss of generality, we set $T_0 = 1.0$, $\rho_0 = 1.0$, and $L = 1.0$. The velocities at the left and right walls are set as $U_L = 0.25$ and $U_R = -0.25$, respectively. The wall temperatures are fixed at $T_w = T_0 = 1.0$, and the diffusive boundary condition is adopted here.

In the calculation, the spatial region is covered by 100 unequally spaced cells with the minimum cell size 0.005. The velocity space is truncated to $[-4.8, 4.8]^3$, and there are 48 uniform velocity mesh points in each direction. The cases with $Kn = 10, 1, 0.1, 0.01$ are computed. The convergence criterion is set to be

$$E^n = \frac{\sum_{i=1}^N \left|W_i^n - W_i^{n-1}\right| V_i}{\sum_i^N \left|W_i^{n-1}\right| V_i} < 1 \times 10^{-6}. \tag{48}$$

Here N is the total number of the discrete cells in the computational domain. As shown in Figure 2, the velocity and temperature profiles computed by the two-step IUGKS match well with the reference solutions. The reference solutions are computed by the conventional iterative scheme (CIS) [33], which reads as

$$\nu(f^n)f^{n+1} + u\cdot\nabla_x f^{n+1} = Q^+(f^n, f^n), \tag{49}$$

where ν is the collision frequency and Q^+ is the gain term of the Boltzmann collision operator. Table 1 shows the convergence history of two-step IUGKS and CIS in the planar Couette flow. We can see that in the highly rarefied regime, both CIS and two-step IUGKS are efficient. However, as Kn decreases, the CIS needs many more steps to get the converged solutions than the two-step IUGKS.

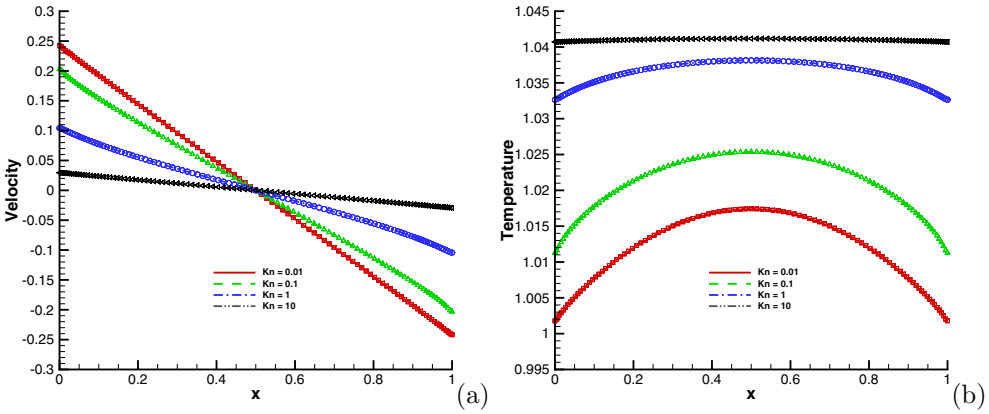

FIG. 2. (a) *Velocity and* (b) *temperature profiles at different Knudsen numbers. The CIS solutions are shown in symbols, and the IUGKS solutions are shown in lines.*

TABLE 1
Efficiency of IUGKS for Couette flow.

State	IUGKS		Two-step IUGKS		
	Steps	Time(s)	Steps	Time(s)	Rate
Kn = 10	9	27	9	28	0.96
Kn = 1	24	66	20	59	1.12
Kn = 0.1	150	407	114	325	1.25
Kn = 0.01	4241	11228	578	1613	6.96

5.2. Fourier flow. In the second case, we study the flow driven by the temperature gradient, and we still consider the full Boltzmann collision operator here. This case is similar to the planar Couette flow but with stationary walls. The temperatures at the left and right walls are set as $T_L = 1.2$ and $T_R = 0.8$, respectively.

The meshes in physical and velocity space and the convergence criterion are the same as the planar Couette flow. The cases at $Kn = 10, 1, 0.1, 0.01$ have been tested. The density and temperature profiles in Figure 3 show that the two-step IUGKS

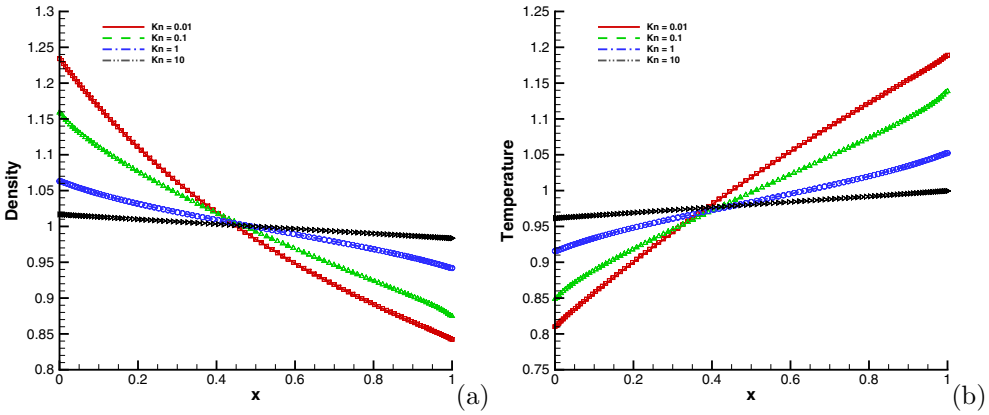

FIG. 3. (a) *Density and* (b) *temperature profiles in different Knudsen numbers. The CIS solutions are shown in symbols, and the IUGKS solutions are shown in lines.*

TABLE 2
Efficiency of IUGKS for planar Fourier flow.

State	IUGKS		Two-step IUGKS		
	Steps	Time(s)	Steps	Time(s)	Rate
Kn = 10	25	69	7	22	3.14
Kn = 1	26	72	19	56	1.29
Kn = 0.1	177	477	107	303	1.57
Kn = 0.01	5026	13331	555	1563	8.53

presents almost identical solutions as the CIS. However, as shown in Table 2, the two-step IUGKS is more efficient than the CIS, especially when the Knudsen number becomes small.

5.3. Lid-driven cavity flow. The lid-driven cavity flow is studied at different Knudsen numbers. The collision model used in this case is the Shakhov model. The cavity has a fixed wall temperature with $T_w = 1.0$. The initial gas inside the cavity is argon gas with density $\rho_0 = 1.0$. The Knudsen number is defined by $\mathrm{Kn} = \mu_0\sqrt{2\pi RT_0}/(2p_0L)$, where $L = 1.0$ is the length of cavity sidewall, and μ_0

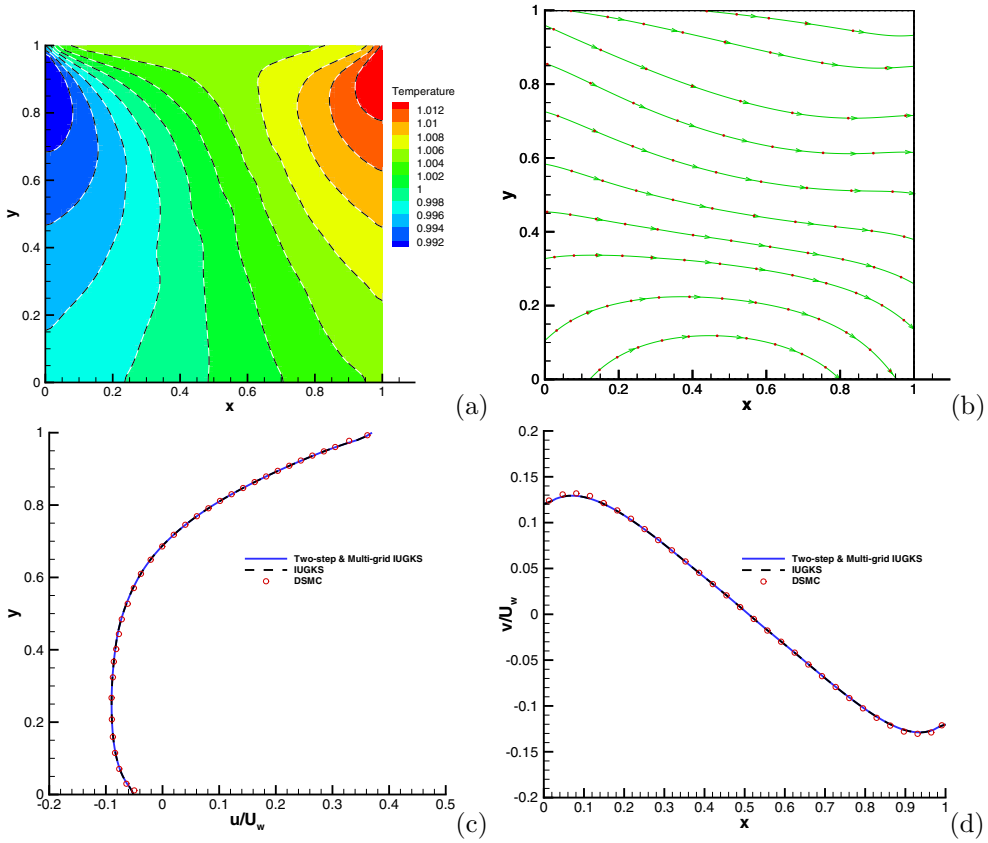

FIG. 4. *Cavity flow at* Kn = 10. (a) *Temperature. Background: two-step multigrid IUGKS; dashed line: IUGKS.* (b) *Heat flux. Line with arrowhead: two-step multigrid IUGKS; circle: IUGKS.* (c) *U-velocity along the central vertical line.* (d) *V-velocity along the central horizontal line.*

is evaluated by the variable hard sphere model with $\omega = 0.81$. The top wall has a velocity of $U_w = 0.148322$ in x direction. A triple V-cycle multigrid solver is used here.

For the case Kn $= 10, 1, 0.075$, the computational domain is discretized by a uniform mesh with 64×64 cells in the physical space. The particle velocity points are 80×80 and 60×60 for Kn $= 10$ and Kn $= 1$, respectively. The trapezoidal integration is used to compute the moments of the distribution function in the two cases, while for the case of Kn $= 0.075$, the Gauss–Hermite quadrature with 28×28 points in velocity space is adopted. The steady state is defined when the mean squared residuals of the conservative variables are reduced to a level being less than 1.0×10^{-6}, where the mean squared residuals are computed by

$$R^n = \sqrt{\frac{\sum_{i=1}^{N} (R_i^n)^2}{N}}. \tag{50}$$

The results for Kn $= 10, 1, 0.075$ are shown in Figures 4, 5, and 6, from which we can see that the results computed by the two-step IUGKS with multigrid solver are identical to those computed by the original IUGKS.

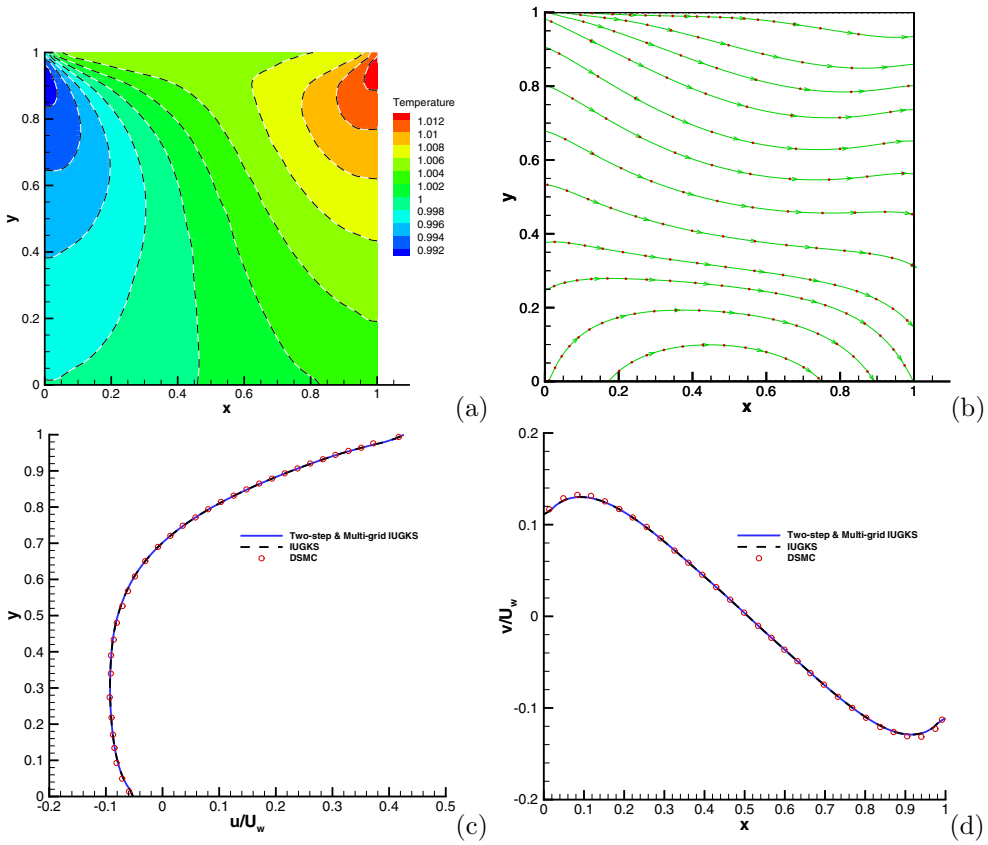

FIG. 5. *Cavity flow at* Kn $= 1$. (a) *Temperature. Background: two-step multigrid IUGKS; dashed line: IUGKS.* (b) *Heat flux. Line with arrowhead: two-step multigrid IUGKS; circle: IUGKS.* (c) *U-velocity along the central vertical line.* (d) *V-velocity along the central horizontal line.*

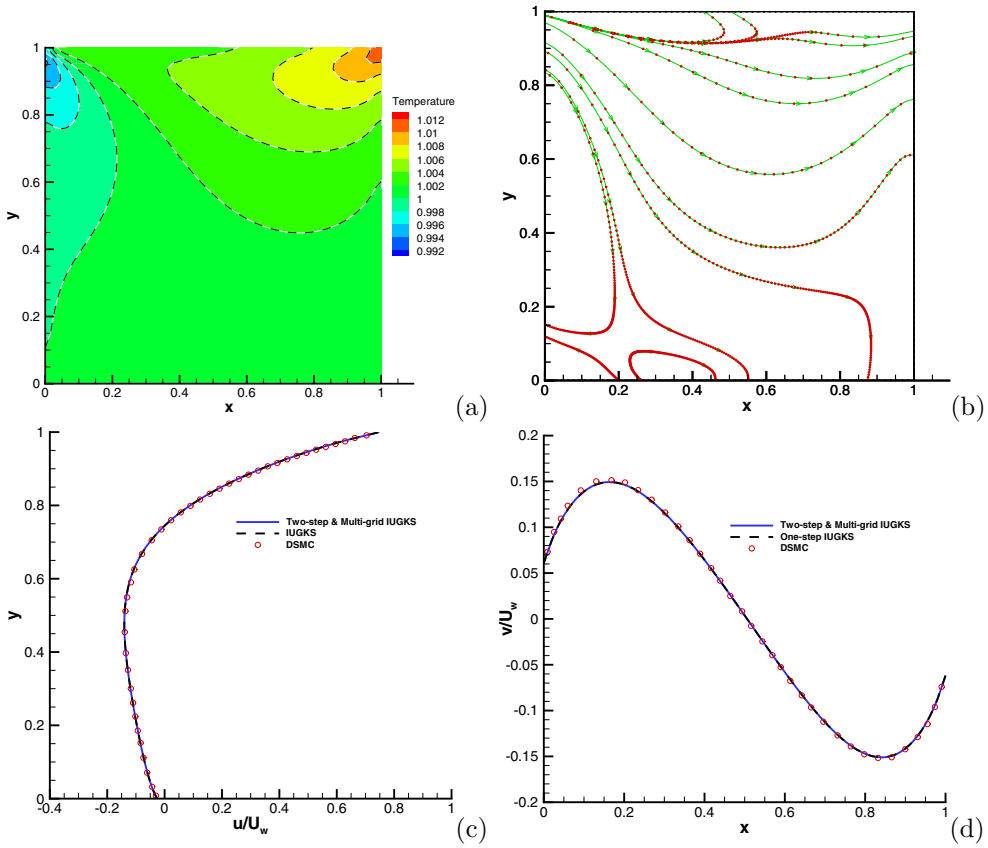

FIG. 6. *Cavity flow at* Kn = 0.075. (a) *Temperature. Background: two-step multigrid IUGKS; dashed line: IUGKS.* (b) *Heat flux. Line with arrowhead: two-step multigrid IUGKS; circle: IUGKS.* (c) *U-velocity along the central vertical line.* (d) *V-velocity along the central horizontal line.*

Two continuum cases at Re = 100 and 1000 are also tested. The mesh is stretched to get a better resolution near the boundaries with $\Delta x_{min} = 0.004$. The particle velocity points are 28×28, and the Gauss–Hermite quadrature is used. The streamlines and the comparison with Ghia's data [40] are plotted in Figure 7. The detailed computational time and acceleration rate in different flow regimes are listed in Table 3. For the rarefied cases at Kn = 10 and 1, the convergence history of the original IUGKS and two-step IUGKS are similar, and the multigrid solver can improve the efficiency of the IUGKS. As the Knudsen number decreases, the two-step acceleration begins to take effect. Especially for the continuum case, the improvement of the efficiency in comparison with the original IUGKS is satisfactory.

5.4. Hypersonic flow past a square cylinder. The last example is the hypersonic flow passing over a square cylinder at Knudsen numbers 1 and 0.1. The Knudsen number is defined by

$$\text{Kn} = \frac{(5-2\omega)(7-2\omega)\mu_\infty\sqrt{2RT_\infty}}{15\sqrt{\pi}p_\infty L}. \tag{51}$$

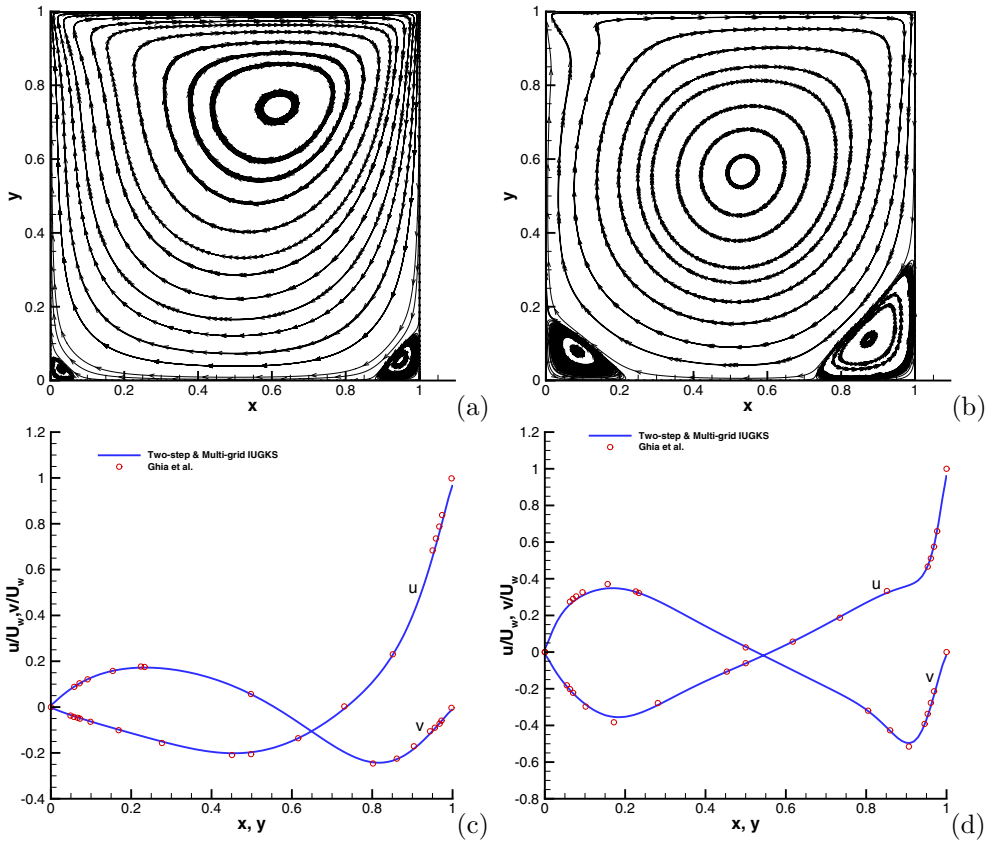

FIG. 7. *Cavity flow at* Re = 100 *(left) and* Re = 1000 *(right).* (a) *and* (b) *Streamlines.* (c) *and* (d) *Velocity along the central lines.*

TABLE 3
Efficiency of different IUGKS for cavity flow.

State	IUGKS		Two-step IUGKS		Two-step & multigrid IUGKS		
	Steps	Time(min)	Steps	Time(min)	Steps	Time(min)	Rate
Kn = 10	80	13.8	80	13.8	33	7.7	1.8
Kn = 1	79	7.7	77	7.6	33	4.4	1.75
Kn = 0.075	169	3.6	51	1.2	20	0.6	6.0
Re = 100	923	19.5	74	1.7	36	1.1	17.7
Re = 1000	3480	73.5	263	6.0	187	5.6	13.1

Here, $L = 1$ is the diameter of the square cylinder, and $\omega = 0.81$. The free streaming argon gas has a speed of Ma = 5 and a temperature $T_\infty = 1$. The temperature of the solid surface of the square cylinder is set to be $T_w = T_\infty$, and the diffusive boundary condition is adopted in the calculations. Due to the symmetry, the solution on half of the physical domain will be calculated.

The computational domain is discretized unequally with $\Delta x_{min} = 0.01$. For the velocity space, 101 uniform discrete velocity points are used. The Newton–Cotes rule is applied here to compute the numerical integration. A two-layer V-cycle multigrid solver is used here. In this hypersonic case, the convergence criterion is set as $R^n < 1 \times 10^{-4}$.

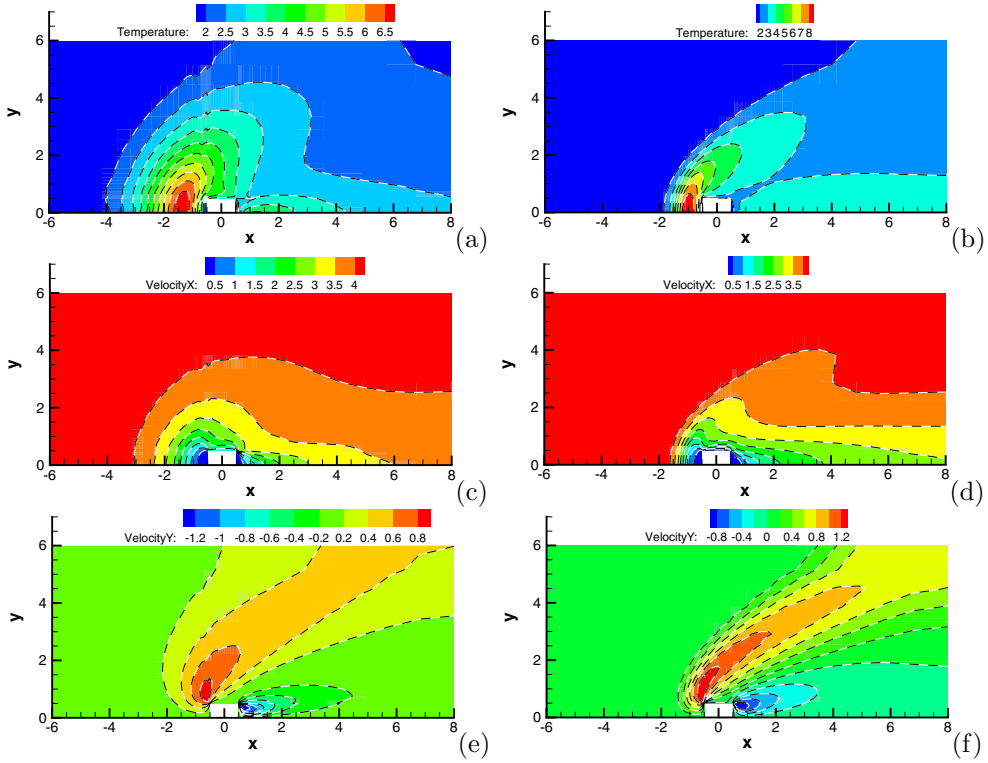

FIG. 8. *Hypersonic flow around a square cylinder at* Kn = 1 *(left) and* Kn = 0.1 *(right).* (a) *and* (b) *Temperature.* (c) *and* (d) *X-velocity.* (e) *and* (f) *Y-velocity. Background: two-step multigrid IUGKS; dashed line: IUGKS.*

TABLE 4
Efficiency of different IUGKS for hypersonic flow around a square cylinder.

State	IUGKS		Two-step IUGKS		Two-step & multigrid IUGKS		
	Steps	Time(min)	Steps	Time(min)	Steps	Time(min)	Rate
Kn = 1	100	21.7	96	20.7	72	19.4	1.1
Kn = 0.1	214	45.6	102	22.2	67	17.8	2.56

The steady-state solutions are presented in Figure 8, and the solutions are compared with the solutions computed by the original IUGKS. The flow variables along the symmetric axis in the upstream are shown in Figure 9. The results from the current two-step IUGKS with a multigrid solver are consistent with the original IUGKS. The detailed efficiency information is shown in Table 4. Since the multigrid method needs to do the calculations on both fine and coarse meshes, even with the same steps, the cost for each time step is higher than that of the other two methods. In the hypersonic rarefied case at Kn = 1, the improvement in efficiency by using the multigrid method is not obvious. In the case of Kn = 0.1, the computational cost with multigrid is reduced by more than two times, which is consistent with the conclusion in the cavity flow.

6. Conclusion. In this paper, a two-step IUGKS is constructed for the steady-state solution in all flow regimes. The full Boltzmann collision operator is also integrated into the implicit scheme. Benefiting from the coupled iterative methods for the

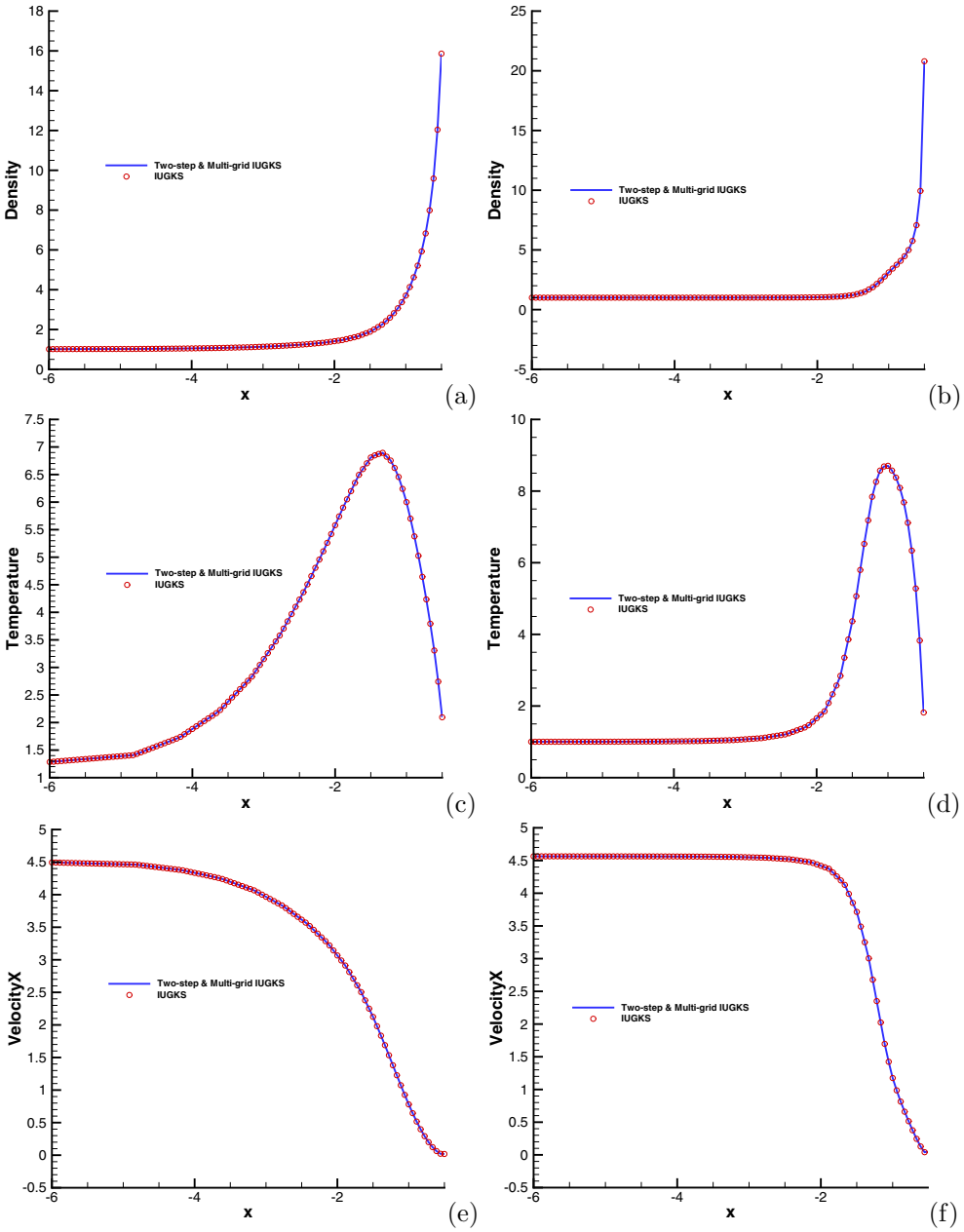

FIG. 9. *Flow variables along the symmetric axis in front of the cylinder at* Kn = 1 *(left) and* Kn = 0.1 *(right).* (a) *and* (b) *Density.* (c) *and* (d) *Temperature.* (e) *and* (f) *U-velocity.*

implicit macroscopic and microscopic equations, the efficiency of the IUGKS can be increased significantly for a steady-state solution. By taking into account the viscous flux in the iterative matrix, the two-step acceleration technique can further improve the efficiency of the original IUGKS, especially in the near continuum and continuum flow regimes. In the current implicit scheme, the LU-SGS and the multigrid methods are used to solve the algebraic systems for the macro-micro equations. Excellent nu-

merical performance has been observed in all test cases, such as Couette flow, Fourier flow, cavity flow, and hypersonic flow passing over a square cylinder. The reasons for the speed-up can be classified into two aspects. In the rarefied regime, the collision term is regular, and the multigrid method can be helpful for the fast convergence of the linear system constructed by the numerical scheme. In the continuum regime, the collision term becomes stiff, and directly solving the linear system will have very low convergence rate. In order to solve such a linear system efficiently, our strategy is to choose a good initial point, which is what we called the two-step acceleration technique in section 3.4. In the first step we solve the continuum equations to get an approximate solution. This solution can be used as an initial point for solving the original linear system. In general, the UKGS provides a general framework. Many commonly used acceleration techniques can be implemented easily into the scheme.

Acknowledgment. We would like to thank Prof. L. Wu for helpful discussions.

REFERENCES

[1] L. Boltzmann, *Lectures on Gas Theory*, Dover, New York, 2012.
[2] P. Bhatnagar, E. Gross, and M.Krook, *A model for collision processes in gases.* I. *Small amplitude processes in charged and neutral one-component systems*, Phys. Rev., 94 (1954), pp. 511–525.
[3] L. H. Holway Jr., *New statistical models for kinetic theory: Methods of construction*, Phys. Fluids 9 (1966), pp. 1658–1673.
[4] E. Shakhov, *Generalization of the Krook kinetic relaxation equation*, Fluid Dyn. 3 (1968), pp. 95–96.
[5] S. Chapman, T. G. Cowling, and D. Burnett, *The Mathematical Theory of Non-uniform Gases: An Account of the Kinetic Theory of Viscosity, Thermal Conduction and Diffusion in Gases*, Cambridge University Press, Cambridge, 1990.
[6] K. Xu, *A gas-kinetic BGK scheme for the Navier–Stokes equations and its connection with artificial dissipation and Godunov method*, J. Comput. Phys., 171 (2001), pp. 289–335.
[7] K. Xu, *Direct Modeling for Computational Fluid Dynamics: Construction and Application of Unified Gas-Kinetic Scheme*, World Scientific, River Edge, NJ, 2015.
[8] G. A. Bird, *Molecular Gas Dynamics and the Direct Simulation of Gas Flows*, Clarendon Press, Oxford, 1994.
[9] L. Mieussens, *Discrete-velocity models and numerical schemes for the Boltzmann-BGK equation in plane and axisymmetric geometries*, J. Comput. Phys., 162 (2000), pp. 429–466.
[10] W. Larsen, J. Morel, and W. Miller, Jr., *Asymptotic solutions of numerical transport problems in optically thick, diffusive regimes*, J. Comput. Phys., 69 (1987), pp. 283–324.
[11] S. Jin, *Efficient asymptotic-preserving (AP) schemes for some multiscale kinetic equations*, SIAM J. Sci. Comput., 21 (1999), pp. 441–454.
[12] A. Klar and C. Schmeiser, *Numerical passage from radiative heat transfer to nonlinear diffusion models*, Math. Models Methods Appl. Sci., 11 (2001), pp. 749–767.
[13] M. Bennoune, M. Lemou, and L. Mieussens, *Uniformly stable numerical schemes for the Boltzmann equation preserving the compressible Navier-Stokes asymptotics*, J. Comput. Phys., 227 (2008), pp. 3781–3803.
[14] S. Jin, *Asymptotic preserving (ap) schemes for multiscale kinetic and hyperbolic equations: A review*, Riv. Math. Univ. Param (N.S.), 3 (2012), pp. 177–216.
[15] G. Dimarco and L. Pareschi, *Numerical methods for kinetic equations*, Acta Numer., 23 (2014), pp. 369–520.
[16] P. Degond and F. Deluzet, *Asymptotic-preserving methods and multiscale models for plasma physics*, J. Comput. Phys., 336 (2017), pp. 429–457.
[17] S. Jin, *Asymptotic-preserving schemes for multiscale physical problems*, Acta Numer., (2022), pp. 1–82.
[18] K. Xu and J.-C. Huang, *A unified gas-kinetic scheme for continuum and rarefied flows*, J. Comput. Phys., 229 (2010), pp. 7747–7764.
[19] J.-C. Huang, K. Xu, and P. Yu, *A unified gas-kinetic scheme for continuum and rarefied flows* II: *Multi-dimensional cases*, Commun. Comput. Phys., 12 (2012), pp. 662–690.
[20] S. Liu, P. Yu, K. Xu, and C. Zhong, *Unified gas-kinetic scheme for diatomic molecular simulations in all flow regimes*, J. Comput. Phys., 259 (2014), pp. 96–113.

[21] C. Liu, K. Xu, Q. Sun, and Q. Cai, *A unified gas-kinetic scheme for continuum and rarefied flows* IV: *Full Boltzmann and model equations*, J. Comput. Phys., 314 (2016), pp. 305–340.
[22] C. Liu and K. Xu, *A unified gas kinetic scheme for continuum and rarefied flows* V: *Multiscale and multi-component plasma transport*, Communications in Computational Physics, 22 (2017), pp. 1175–1223.
[23] W. T. Taitano, D. A. Knoll, L. Chacón, J. M. Reisner, and A. K. Prinja, *Moment-based acceleration for neutral gas kinetics with BGK collision operator*, J. Comput. Theor. Transp., 43 (2014), pp. 83–108.
[24] L. Chacon, G. Chen, D. A. Knoll, C. Newman, H. Park, W. Taitano, J. A. Willert, and G. Womeldorff, *Multiscale high-order/low-order (HOLO) algorithms and applications*, J. Comput. Phys., 330 (2017), pp. 21–45.
[25] W. Su, L. Zhu, P. Wang, Y. Zhang, and L. Wu, *Can we find steady-state solutions to multiscale rarefied gas flows within dozens of iterations?*, J. Comput. Phys., 407 (2020), 109245.
[26] L. Zhu, X. Pi, W. Su, Z.-H. Li, Y. Zhang, and L. Wu, *General synthetic iterative scheme for nonlinear gas kinetic simulation of multi-scale rarefied gas flows*, J. Comput. Phys., 430 (2021), 110091.
[27] Y. Zhu, C. Zhong, and K. Xu, *Implicit unified gas-kinetic scheme for steady state solutions in all flow regimes*, J. Comput. Phys., 315 (2016), pp. 16–38.
[28] Y. Zhu, C. Zhong, and K. Xu, *Unified gas-kinetic scheme with multigrid convergence for rarefied flow study*, Phys. Fluids, 29 (2017), 096102.
[29] Y. Zhu, C. Zhong, and K. Xu, *An implicit unified gas-kinetic scheme for unsteady flow in all Knudsen regimes*, J. Comput. Phys., 386 (2019), pp. 190–217.
[30] R. Chen and Z. Wang, *Fast, block lower-upper symmetric Gauss-Seidel scheme for arbitrary grids*, AIAA J., 38 (2000), pp. 2238–2245.
[31] F. Filbet and S. Jin, *A class of asymptotic-preserving schemes for kinetic equations and related problems with stiff sources*, J. Comput. Phys., 229 (2010), pp. 7625–7648.
[32] L. Pareschi and G. Russo, *Numerical solution of the boltzmann equation* I: *Spectrally accurate approximation of the collision operator*, SIAM J. Numer. Anal., 37 (2000), pp. 1217–1245.
[33] L. Wu, C. White, T. J. Scanlon, J. M. Reese, and Y. Zhang, *Deterministic numerical solutions of the Boltzmann equation using the fast spectral method*, J. Comput. Phys., 250 (2013), pp. 27–52.
[34] R. Yuan, S. Liu, and C. Zhong, *A multi-prediction implicit scheme for steady state solutions of gas flow in all flow regimes*, Commun. Nonlinear Sci. Numer. Simul., 92 (2021), 105470.
[35] S. Yoon and A. Jameson, *Lower-upper symmetric-Gauss-Seidel method for the Euler and Navier-Stokes equations*, AIAA J. 26 (1988), pp. 1025–1026.
[36] D. Sharov, K. Nakahashi, D. Sharov, and K. Nakahashi, *Reordering of 3-D hybrid unstructured grids for vectorized LU-SGS Navier-Stokes computations*, in Proceedings of the 13th Computational Fluid Dynamics Conference, 1997, pp. 1997–2002.
[37] W. L. Briggs, V. E. Henson, and S. F. McCormick, *A Multigrid Tutorial*, SIAM, Philadelphia, 2000.
[38] A. Brandt and O. E. Livne, *Multigrid Techniques:* 1984 *Guide with Applications to Fluid Dynamics*, Revised Edition, SIAM, 2011.
[39] U. Trottenberg, C. W. Oosterlee, and A. Schuller, *Multigrid*, Elsevier, New York, 2000.
[40] U. Ghia, K. N. Ghia, and C. Shin, *High-Re solutions for incompressible flow using the Navier-Stokes equations and a multigrid method*, J. Comput. Phys., 48 (1982), pp. 387–411.